Journal of Applied Electrochemistry **29**: 1409–1416, 1999.

Modelling of performance of PEM fuel cells with conventional and interdigitated flow fields

A. KAZIM, H.T. LIU and P. FORGES
University of Miami, Department of Mechanical Engineering, Coral Gables, FL 33124, USA

Received 22 October 1998; accepted in revised form 11 May 1999

Key words: flow field, fuel cell, interdigitated flow field, modelling, PEM fuel cell

Abstract

A simple mathematical model is developed to investigate the superiority of the interdigitated flow field design over the conventional one, especially in terms of maximum power density. Darcy's equation for porous media and the standard diffusion equation with effective diffusivity are used in the gas diffuser, and a coupled boundary condition given by the Butler–Volmer equation is used at the catalyst layer interface. The performance of PEM fuel cells with a conventional flow field and an interdigitated flow field is studied with other appropriate boundary conditions. The theoretical results show that the limiting current density of a fuel cell with an interdigitated flow field is about three times the current density of a fuel cell with a conventional flow field. The results also demonstrate that the interdigitated flow field design can double the maximum power density of a PEM fuel cell. The modelling results compared well with experimental data in the literature.

List of symbols

C	oxygen concentration (mol cm^{-3})
C_o	Inlet oxygen concentration (mol cm^{-3})
C_{ref}	reference concentration of oxygen (mol cm^{-3})
D_{eff}	effective diffusion coefficient (cm^2 s^{-1})
F	Faraday's constant (96 487 C mol^{-1})
H	gas diffuser depth (cm)
$\bar{I}$	average current density (A cm^{-2})
I_0	exchange current density (A cm^{-2})
$I(x)$	local current density along the electrode (A cm^{-2})
k_p	hydraulic permeability (cm^2)
L	electrode width (cm)
L_1	electrode entrance width (cm)
L_2	electrode entrance and collector base width (cm)
n	number of electrons involved in the electrochemical reaction
P	cell total pressure (atm)
P_e	exit pressure (atm)
P_{in}	inlet pressure (atm)
$\mathscr{P}$	fuel cell overall power density (W cm^{-2})
$\mathscr{R}$	gas constant (82.06 cm^3 atm mol^{-1} K^{-1})
R	membrane resistance (Ω cm^2)
T	fuel cell operating temperature (°C)
u, v	components of the fluid velocity (cm s^{-1})
V_{cell}	fuel cell potential (V)
V_{oc}	open circuit voltage (V)
x, y	space variables (cm)
X	mole fraction of oxygen, dimensionless

Greek symbols

μ	pore liquid viscosity (kg cm^{-1} s^{-1})
η	electrode overpotential (V)

Subscripts and superscripts

cell	fuel cell
e	exit
in	inlet
oc	open circuit
ref	reference

1. Introduction

In a PEM fuel cell the limiting current density, and thus the maximum power, are often determined by the maximum mass transfer rates of the reactants to the reaction sites. Mass-transport limitations depend on the porosity and tortuosity of porous electrodes and the amount of liquid water they contain. If the product water is not effectively removed from a fuel cell, flooding occurs, which prevents the effective transfer of reactants to the catalyst layer. As reported by Yi and Nguyen [1], when a fuel cell accumulates too much water at high current densities, about a third of the electrode surface area is not utilized. To overcome such mass-transport limitations in porous electrodes, new flow fields have recently been developed. One of them is called the interdigitated flow

field, which consists of dead-end gas channels that force the gases through the porous electrodes.

Wilson et al. [2], Ledjeff et al. [3] and later Nguyen [4] have studied interdigitated flow fields, but modelling efforts in this area are very limited. Yi and Nguyen [5] have presented some preliminary results. The objective of this study is to develop a simple mathematical model of PEM fuel cells with different flow fields, particularly to compare the performance of PEM fuel cells with interdigitated and conventional flow fields. Finally, the modelling results are compared with experimental data available in the literature.

2. Model formulation

It has been demonstrated that the main mass transport limitations in PEM fuel cells occur within electrode layers [4]. It has been found that the kinetics of the oxygen reduction reaction at the cathode is at least five orders of magnitude slower than hydrogen oxidation [6]. Therefore, we focus attention on oxygen gas transport through the cathode region of PEM fuel cells.

As depicted in Figure 1(a), in the cathode gas channel of a conventional flow field, air flows parallel to the gas

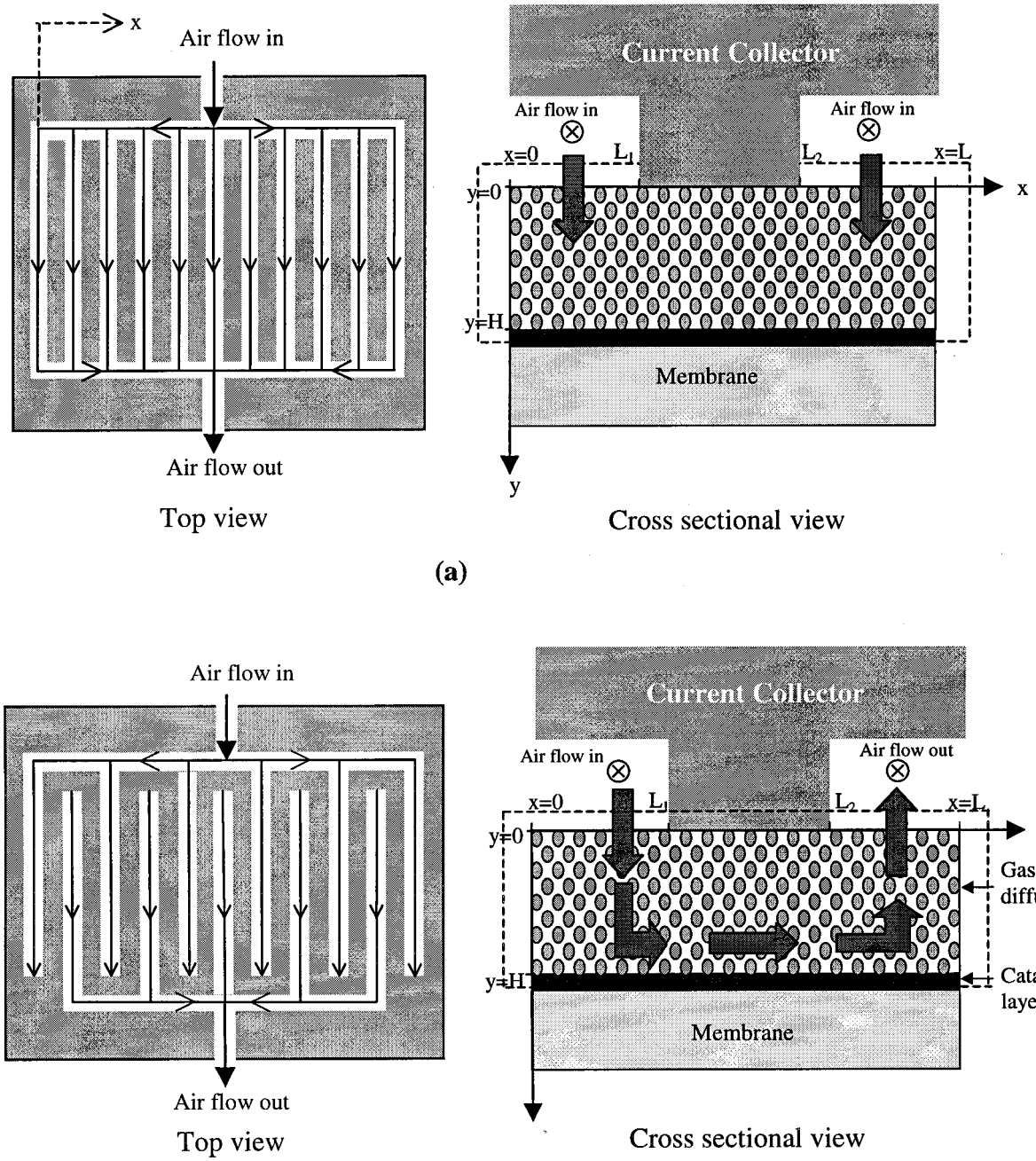

Fig. 1. Schematic diagram of PEM fuel cell with conventional flow field (a) and interdigitated flow field (b). ⊗ Indicates that air is flowing perpendicular to the page and toward the reader (z-axis direction).

diffusion layer. The predominant mechanism of oxygen transfer to the catalyst layer is diffusion. In the interdigitated flow field shown in Figure 1(b), flow channels are dead-ended forcing air to flow through the porous diffusion layer. The diffusive mass transfer mechanism is changed into a forced convective mass transfer in the interdigitated flow field, which causes limiting current density and maximum power density increase significantly.

In developing the model, the following assumptions were used: the gas mixture is incompressible; the fuel cell is isothermal; the gas mixture is an ideal gas; the effective diffusion coefficient of oxygen in the porous media is constant; oxygen is chemically reduced at the catalyst surface instead of throughout the catalyst layer; and the cell over-potential on the anode side is negligible.

3. Governing equations and boundary conditions

As shown in Figure 1, $x = 0$ is the middle of any cathode channel, and $x = L$ is the middle of the adjacent channel. The current collector is in contact with the porous diffusion layer between $x = L_1$ and $x = L_2$. At the interface of the gas diffuser with the gas channels, $y = 0$, and at the interface between the gas diffuser and the catalyst layer $y = H$. The domain within which all the subsequent equations are valid is therefore the rectangle $(x, y) = (0, L) \times (0, H)$.

The governing equations are the continuity equation, Darcy's law and the equation of conservation of species given below:

$$\frac{\partial u}{\partial x} + \frac{\partial v}{\partial y} = 0 \tag{1}$$

$$u = -\frac{k_p}{\mu}\left(\frac{\partial P}{\partial x}\right) \qquad v = -\frac{k_p}{\mu}\left(\frac{\partial P}{\partial y}\right) \tag{2}$$

$$u\frac{\partial C}{\partial x} + v\frac{\partial C}{\partial y} = D_{\text{eff}}\left(\frac{\partial^2 C}{\partial x^2} + \frac{\partial^2 C}{\partial y^2}\right) \tag{3}$$

From Equations 1 and 2, the following Laplace's equation for pressure is obtained:

$$\frac{\partial^2 P}{\partial x^2} + \frac{\partial^2 P}{\partial y^2} = 0 \tag{4}$$

The governing equations are identical for both conventional and interdigitated flow fields. The difference exists in the boundary conditions for P and C at the interface between the gas flow channels and the gas diffuser. In all other boundaries, the two types of flow fields have the same boundary conditions. The boundary conditions for both flow fields are summarized below:

For $0 \le y \le H$, and $x = 0$ or $x = L$

Conventional	Interdigitated
$\begin{cases} \dfrac{\partial P}{\partial x} = 0 \\ \dfrac{\partial C}{\partial x} = 0 \end{cases}$	$\begin{cases} \dfrac{\partial P}{\partial x} = 0 \\ \dfrac{\partial C}{\partial x} = 0 \end{cases}$

(5a)

For $L_1 \le x \le L_2$, and $y = 0$

$$\begin{cases} \dfrac{\partial P}{\partial y} = 0 \\ \dfrac{\partial C}{\partial y} = 0 \end{cases} \qquad \begin{cases} \dfrac{\partial P}{\partial y} = 0 \\ \dfrac{\partial C}{\partial x} = 0 \end{cases} \tag{5b}$$

For $0 < x < L$, and $y = H$

$$\begin{cases} \dfrac{\partial P}{\partial y} = 0 \\ \dfrac{\partial C}{\partial y} = -\phi C \end{cases} \qquad \begin{cases} \dfrac{\partial P}{\partial y} = 0 \\ \dfrac{\partial C}{\partial y} = -\phi C \end{cases} \tag{5c}$$

For $0 < x < L_1$, and $y = 0$

$$\begin{cases} P = P_{\text{in}} \\ C = C_{\text{ref}} \end{cases} \qquad \begin{cases} P = P_{\text{in}} \\ C = C_{\text{ref}} \end{cases} \tag{5d}$$

For $L_2 < x < L$, and $y = 0$

$$\begin{cases} P = P_{\text{in}} \\ C = C_{\text{ref}} \end{cases} \qquad \begin{cases} P = P_{\text{e}} \\ \dfrac{\partial C}{\partial y} = 0 \end{cases} \tag{5e}$$

where ϕ is the fuel cell electrostatic potential and can be determined from the following Butler–Volmer expression, which has been widely used,

$$\phi = \frac{I_0}{nFD_{\text{eff}}C_{\text{ref}}}\exp\left(\frac{\alpha F}{\mathscr{R}T}\eta\right) \tag{6}$$

where C_{ref} is the inlet oxygen concentration.

Once the concentration in the gas diffuser is determined, the local current density generated at the reaction surface, where $y = H$ along the x-direction $I(x)$, is calculated using the following expressions:

$$I(x) = nFD_{\text{eff}}\left.\frac{\partial C}{\partial y}\right|_{y=H} \tag{7}$$

The average current density along the reaction surface is then determined by

$$\bar{I} = \frac{1}{L}\int_0^L I(x)\mathrm{d}x \tag{8}$$

Neglecting the overpotential on the anode side, the cell potential is calculated as

$$V_{\text{cell}} = V_{\text{oc}} - \eta - \bar{I}R \tag{9}$$

where the ohmic resistance, R, is set to a constant value of $0.16\ \Omega\text{cm}^2$ throughout the electrode, which is a typical value measured in our experiments. To concentrate on the comparison of performance of the two types of flow fields, constant values of the open circuit voltage V_{oc} are used. The overall power density of the cell is then calculated by using:

$$\mathscr{P} = V_{\text{cell}}\bar{I} \tag{10}$$

The model parameters used for our base case and the cathode physical properties are listed in Table 1.

In the solution procedure, the overpotential η is used as an input parameter. For each value of η, a current density can be obtained, thus the polarization curve can be produced.

In the operation of fuel cells, the value of P_{e} can be determined by changing the backpressure. When the inlet pressure is kept constant, we can obtain any predetermined stoichiometric flow rate of oxygen by adjusting the backpressure valve. A similar process is used in the numerical simulation: the boundary condition of P_{e} is determined by an iterative process to satisfy the predetermined stoichiometric flow rate of oxygen. We may also preset the pressure-drop to compare our modelling result with the experimental result obtained by Nguyen [4], since pressure drop, rather than stoichiometric ratio, was reported in their paper.

4. Numerical procedure

Governing Equations 3 and 4 are solved by a finite difference method. Derivatives are approximated by a central-, forward- or backward-difference representation, accurate to the second order in the x- and y-directions. The x-axis is discretized by:

Table 1. Physical parameters and properties in the channel and the electrode

Quantity	Value	Source
Operating temperature, T/°C	85.0	Typical value
Operating pressure, P/atm	5.0	Typical value
Cathode width, L/cm	0.18	Typical value
Cathode height, H/cm	0.02	Typical value
Effective diffusion coefficient, $D_{\text{eff}}/\text{cm}^2\ \text{s}^{-1}$	0.0125	calculated
Exchange current density, $I_0/\text{A cm}^{-2}$	0.01	[8]
Number of electrons, n	4	
Open circuit voltage, V_{oc}/V	1.1	[8]
Transfer coefficient, α dimensionless	2	
Reference oxygen concentration $C_{\text{ref}}/\text{mol cm}^{-3}$	3.57×10^{-5}	calculated
Ohmic resistance $R/\Omega\ \text{cm}^2$	0.285	[8]
Hydraulic permeability, k_{p}/cm^2	1.0×10^{-8}	[7]
Fluid viscosity, $\mu/\text{kg cm}^{-1}\ \text{s}^{-1}$	0.21×10^{-6}	[8]

M_1 points

$$x_{1\le i\le M_1} = (i-1)\frac{L_1}{M_1 - 1}$$
between $x = 0$ and $x = L_1$

M_2 points

$$x_{1\le i\le M_2} = L_1 + (i-1)\frac{L_2 - L_1}{M_2 - 1}$$
between $x = L_1$ and $x = L_2$

M_3 points

$$x_{1\le i\le M_3} = L_2 + (i-1)\frac{L - L_2}{M_3 - 1}$$
between $x = L_2$ and $x = L$

The y-axis is uniformly discretized by:

$$N \text{ points } y_{1\le j\le N} = (j-1)\frac{H}{N-1}$$

Four steps are necessary to obtain the overall power density of the cell, as a function of η. (i) Pressure field within the cathode is computed by solving $\nabla^2 P = 0$ with the appropriate boundary conditions of a fuel cell equipped with an interdigitated flow field. (ii) From the knowledge of P and by using Darcy's law (Equation 2), both components of the gas velocity vector are calculated. (iii) Once step two is accomplished, the species equation is solved to obtain the oxygen concentration distribution in the cathode gas diffuser. (iv) Finally, the molar flux of oxygen, the average current density, the overall polarization and power density of the fuel cell are computed.

The numerical scheme implemented should respect conservation laws. Because we used a finite difference method that does not enforce the conservation laws automatically, the following constraint was checked for convergence for the interdigitated flow field.

$$\begin{aligned}
&\int_0^{L_1}\left[C(x,0)v(x,0) - D_{\text{eff}}\frac{\partial C}{\partial y}\bigg|_{y=0}\right]\mathrm{d}x \\
&= \int_{L_2}^{L}\left[-C(x,0)v(x,0) + D_{\text{eff}}\frac{\partial C}{\partial y}\bigg|_{y=0}\right]\mathrm{d}x \\
&+ \int_0^{L} D_{\text{eff}}\frac{\partial C}{\partial y}\bigg|_{y=H}\mathrm{d}x + \frac{I_0}{nFC_{\text{ref}}}\exp\left(\frac{\alpha F}{\mathscr{R}T}\eta\right)\int_0^{L} C(x,H)\mathrm{d}x
\end{aligned} \tag{11}$$

This equation requires that the number of moles of O_2 entering the domain per unit time from the boundary $(0 < x < L_1, y = 0)$ equal the sum of: (i) the number of

moles of O_2 leaving the domain per unit of time from the boundary ($L_2 < x < L, y = 0$) and (ii) the number of moles of oxygen chemically reduced per unit time at the reaction surface ($0 < x < L, y = H$).

5. Results and discussion

Figure 2 presents the oxygen concentration distributions at various values of overpotential η in a conventional

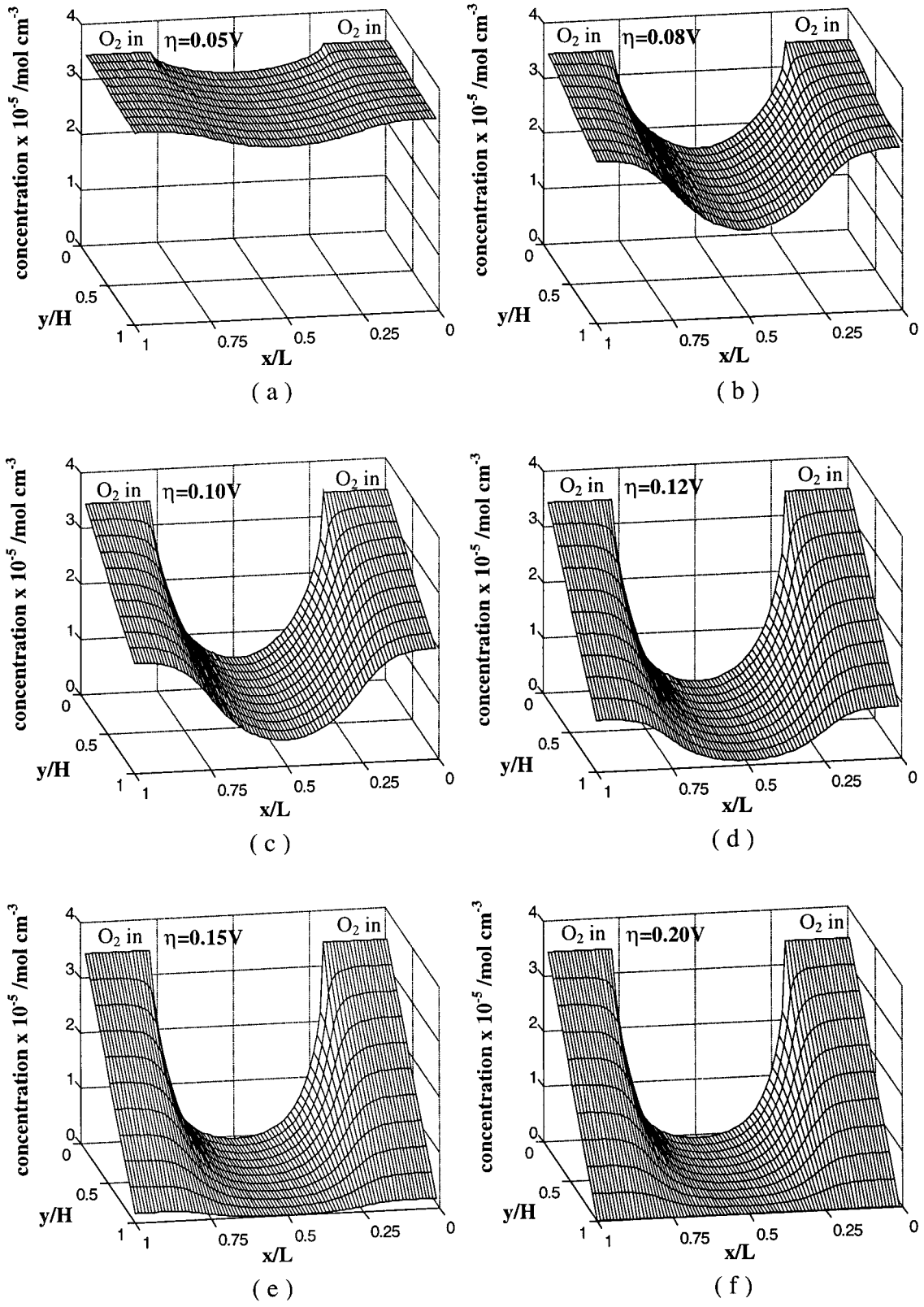

Fig. 2. Oxygen concentration distribution in the gas diffuser with conventional flow field at different values of over-potential, η. $P = 5$ atm and $T = 85\ ^\circ C$.

flow field. Since diffusion is the only mass transfer mechanism, oxygen concentration decreases linearly in the direction toward the reaction surface. Furthermore, as expected, low concentrations are obtained both at location far from the source of O_2 (namely at the boundary $L_1 < x < L_2, y = 0$) and on the reaction surface where the oxygen is chemically reduced ($0 < x < L$, $y = H$). It follows that at point $(x = (L_1 + L_2)/2$, $y = H), C$ takes its lowest value. By increasing η from 0.05 to 0.2 V, more oxygen is consumed along the reaction surface. At any point where $\eta > 0.2$ V, oxygen will be fully depleted at the reaction surface and the current density will reach its limiting value.

In the case of an interdigitated flow field, the pressure distribution is determined first, and Figure 3 shows a typical result. Next, by applying Darcy's law, the gas velocity field is obtained. Figure 4 shows a typical result of a velocity field corresponding to the conditions in Figure 3. After the result of velocity distribution is obtained, the oxygen concentration distribution can be determined.

Figure 5 presents the oxygen concentration distribution in the gas diffusion layer of an interdigitated flow field at various values of overpotential. To facilitate comparison, the overpotential values are the same as those used in the conventional flow field case.

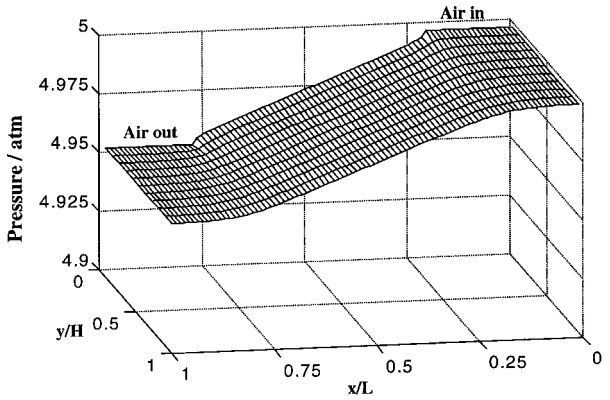

Fig. 3. Pressure drop in the gas diffuser with interdigitated flow field.

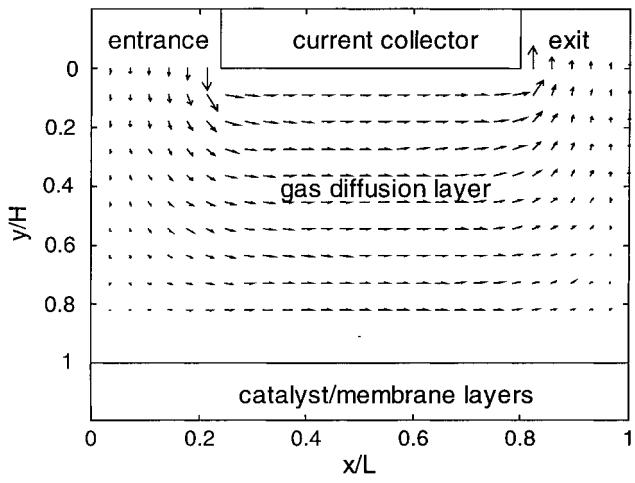

Fig. 4. Velocity vectors in the gas diffuser with interdigitated flow field.

Figure 6 shows local current density $I(x)$ as a function of a normalized variable x, for both conventional and interdigitated flow fields. It is evident from Figure 6 that local current densities are much higher in an interdigitated flow field. When operating a fuel cell with an interdigitated flow field, it appears that the local current density is a maximum near $x = L_1$. Figure 4 indicates that the velocity of oxygen flowing into the porous media is increasingly high as it comes close to the current collector. Higher velocity carries larger amounts of oxygen to the reaction surface; thus, a higher current density is achieved.

The interdigitated flow field outperforms the conventional flow field, especially at high current densities. The rate of oxygen consumption increases as current density increases. The conventional flow field cannot provide a high oxygen transfer rate because of the diffusion limitations, whereas an interdigitated flow field can supply oxygen at a much higher rate by forced convection.

Figure 7 shows a typical set of polarization curves, and Figure 8 shows the corresponding power density curves. It is obvious that the interdigitated flow field significantly outperforms the conventional one. The limit current density for a fuel cell with an interdigitated flow field is approximately three times that for a fuel cell with a conventional flow field, and the maximum power is approximately doubled.

To verify our model, we compared results with experimental data obtained by Nguyen [4]. Figure 9 shows the comparison of the simulated power density curves with the corresponding experimental values. Both the modelling results and the experimental data show the same factor of limiting current density increase when interdigitated flow field is used. We also noticed that the model always overpredicts power density, especially in a conventional flow field. This is because our model neglects mass transfer resistance in the catalyst layer, and assumes the catalyst layer to be a surface.

6. Conclusions

We developed a simple two-dimensional steady state model of PEM fuel cells with different flow fields. Specifically, fuel cells with interdigitated and conventional flow fields were studied. Through proper handling of the boundary condition at the interface between the gas diffusion layer and the catalyst layer, we were able to solve the Butler–Volmer equation together with the transport equations. Taking the overpotential on the cathode side as a parameter, we have obtained polarization and power density curves as a function of current density for both flow fields. The modelling results show that the mass transfer enhancement of the interdigitated flow field has a significant effect on fuel cell performance. When the mode of mass transfer is changed from

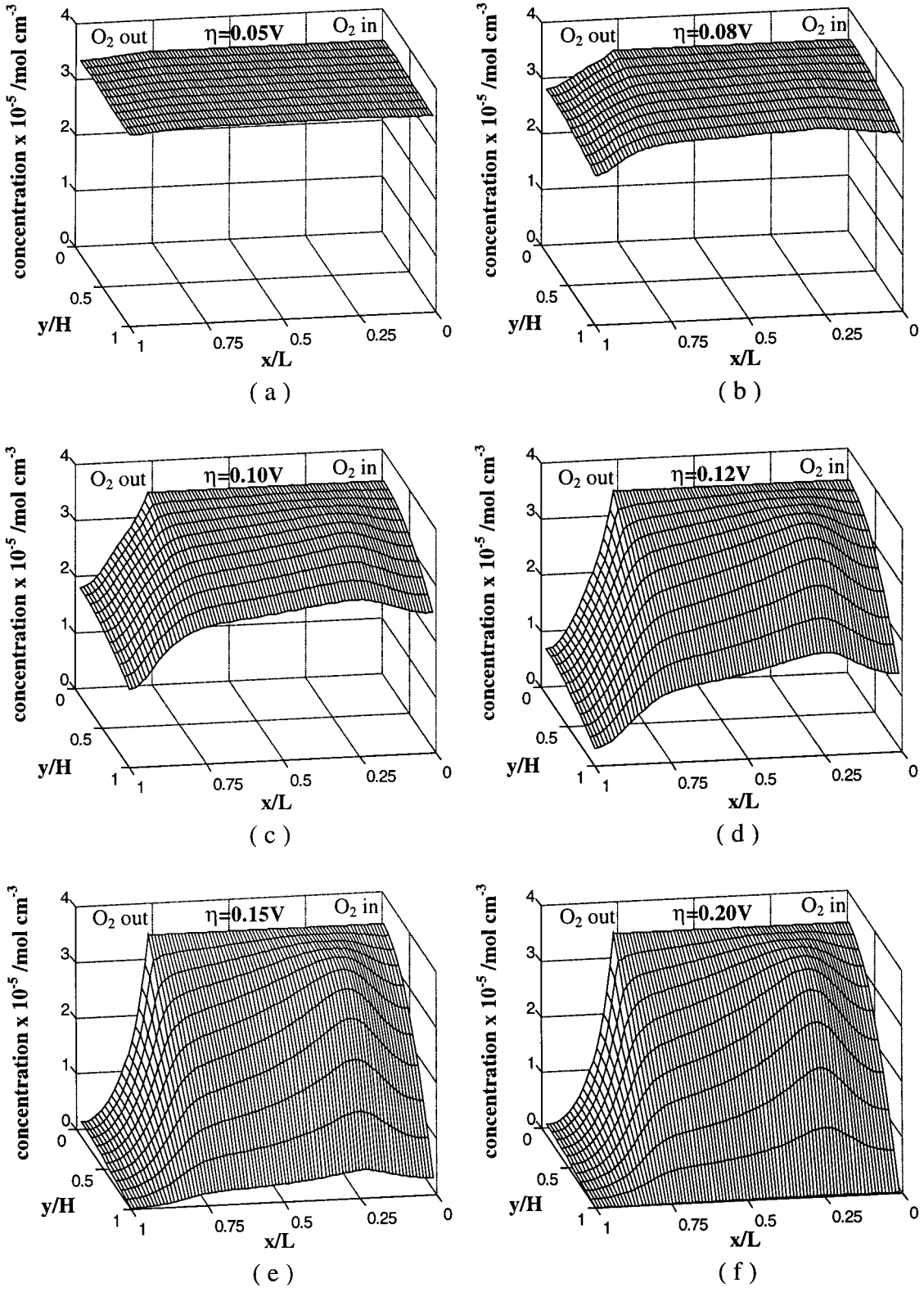

Fig. 5. Oxygen concentration distribution in the gas diffuser with interdigitated flow field at different values of overpotential, η. $P = 5$ atm and $T = 85\ ^{\circ}C$.

diffusion to forced convection, the limit current density increases threefold and the maximum power doubles. This is obviously very important in fuel cell applications, especially for automotive applications, where weight and power density are of primary importance.

The numerical values of the results obtained in this paper obviously depend on the model parameters selected. However, the general conclusions from this model are valid for most reasonable operating conditions. In summary, our modelling results demonstrate

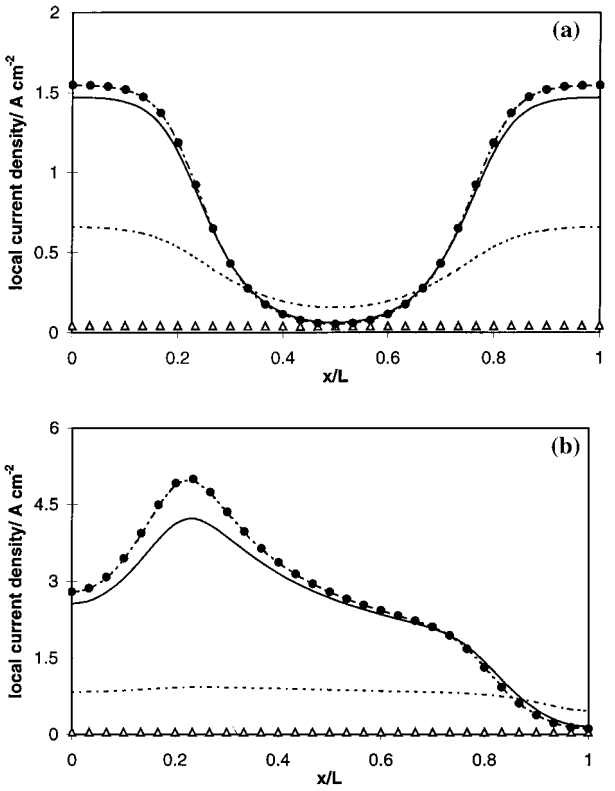

Fig. 6. Local current density in the gas diffuser with conventional flow field (a) and with interdigitated flow field (b) at different values of overpotential, η: (△) 0.10, (- - - -) 0.12, (——) 0.15 and (- · - ·) 0.20 V. (●) C = 0.

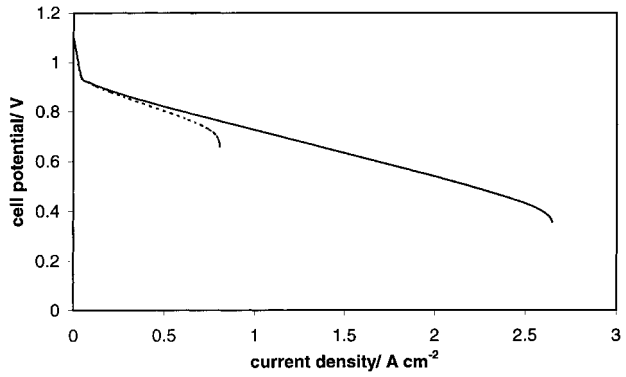

Fig. 7. Polarization curves of fuel cells with conventional (- - - -) and interdigitated (——) flow fields.

the superiority of interdigitated flow fields over conventional ones. The modelling results also compare well with experimental data in the literature.

Acknowledgement

The authors gratefully acknowledge the financial supports of the US Department of Energy's Hydrogen Program and CARAT Program.

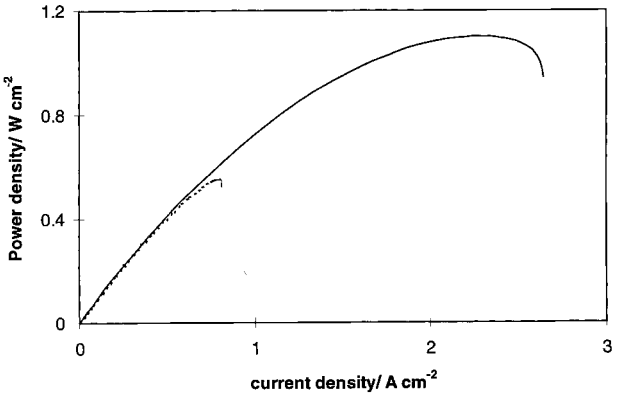

Fig. 8. Power density curves of fuel cells with conventional (- - - -) and interdigitated (——) flow fields.

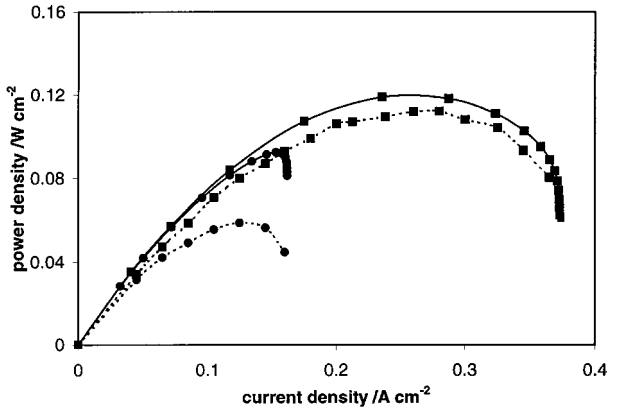

Fig. 9. Comparison of power density curves between experimental (dotted curves) and modelling (full curves) results at $P = 1$ atm, and $T = 25\,^{\circ}\mathrm{C}$. Flow field: (●) conventional and (■) interdigited.

References

1. J.S. Yi and T.V. Nguyen, *Electrochem. Soc. Proc.* **23** (1995) 66–75.
2. M.S. Wilson, T.E. Springer, J. Davey and S. Gottesfeld, *Electrochem. Soc. Proc.* **23** (1995) 115–26.
3. K. Ledjeff, A. Heinzel, F. Mahlendorf and V. Peinecke, *Dechema Monographien* **128** (1993) 103.
4. T.V. Nguyen, *J. Electrochem. Soc.* **143** (1996) L103–L105.
5. J.S. Yi and T.V. Nguyen, *Electrochem. Soc. Meeting*, Extended Abstract. **189** (1997) 228.
6. T.E. Springer, T.A. Zawodzinski and S. Gottesfeld, *J. Electrochem. Soc.* **143** (1996) 587–99.
7. D. Bernardi and M. Verbrugge, *J. Electrochem. Soc.* **139** (1992) 2477–91.
8. T.E. Springer, T.A. Zawodzinski and S. Gottesfeld, *J. Electrochem. Soc.* **138** (1991) 2334–42.